Journal of Colloid and Interface Science 561 (2020) 275–286

Contents lists available at ScienceDirect

Journal of Colloid and Interface Science

journal homepage: www.elsevier.com/locate/jcis

The role of fluoroaluminate complexes on the adsorption of fluoride onto hydrous alumina in aqueous solutions

Jui-Yen Lin [a], Yung-Long Chen [b], Xin-Ya Hong [b], Chinpin Huang [b,*], C.P. Huang [c]

[a] Department of Chemical Engineering, National Cheng Kung University, Tainan 701, Taiwan
[b] Institute of Environmental Engineering, National Chiao Tung University, Hsinchu 300, Taiwan
[c] Department of Civil and Environmental Engineering, University of Delaware, Newark, DE 19716, United States

GRAPHICAL ABSTRACT

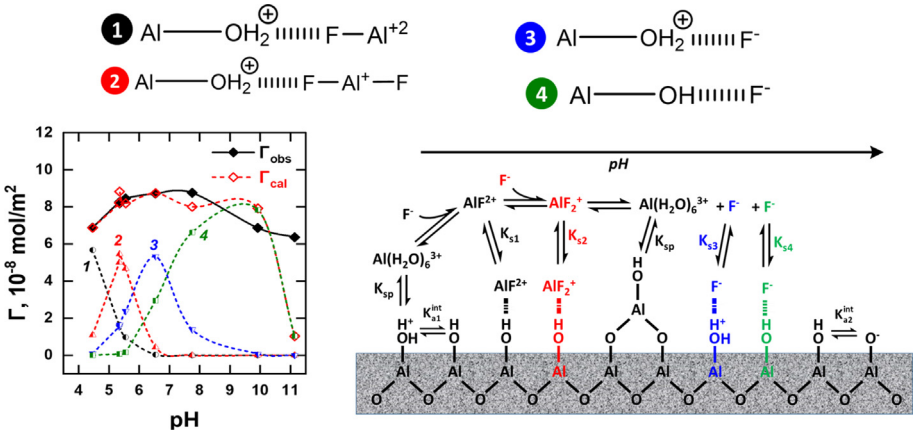

ARTICLE INFO

Article history:
Received 19 August 2019
Revised 14 October 2019
Accepted 19 October 2019
Available online 6 November 2019

Keywords:
Fluoride
γ-Al_2O_3
Fluoroaluminate complexes
Adsorption
Surface complexation
Surface acidity

ABSTRACT

Activated alumina (AA) has been extensively applied in the defluorination of industrial wastewaters and groundwater. Although the dissolution of AA due to formation of fluoroaluminate complexes (AlF_x^{3-x}), especially in acidic condition, has been observed, its role on fluoride uptake by alumina has not been discussed in any previous literature, most of which consider F^- as the sole adsorbed species. The present study described the effect of fluoroaluminate complexes on fluoride adsorption onto alumina. Results indicated that fluoroaluminate complexes, major fluoride species at pH < 6, were responsible for total fluoride adsorbed. Free fluoride ions were adsorbed mainly in the alkaline pH region, e.g., pH > 6. The dissolution of AA during defluorination was measured and analyzed by the thermodynamic solubility model. The surface concentration of F^- and AlF_x^{3-x} were calculated considering electrostatic interactions. Characterization of fluoride-laden AA by XPS revealed that the fraction of surface Al-F species decreased with pH, which suggested the transition of the surface fluorinated species to that of free fluoride ions. The stability constants of four surface complexes, namely, $\underline{Al}OH\text{-}FAl^{2+}$, $\underline{Al}OH\text{-}F_2Al^{+}$, $\underline{Al}OH_2^{+}\text{-}F^{-}$ and $\underline{Al}OH\text{-}F^{-}$, were $10^{6.88}$, $10^{5.36}$, $10^{2.72}$ and $10^{2.36}$, respectively. Obviously fluoroaluminate complexes exhibited stronger chemical bonds with the surface hydroxy species than free fluoride.

* Corresponding author.
E-mail addresses: jylin@udel.edu (J.-Y. Lin), ylchena@tsma.com (Y.-L. Chen), cphuang@nctu.edu.tw (C. Huang), huang@udel.edu (C.P. Huang).

https://doi.org/10.1016/j.jcis.2019.10.085
0021-9797/

1. Introduction

Groundwater in many regions of the globe have suffered from excess fluoride due to mineral dissolution, deposition of gaseous and particulate fluoride, and contamination from industrial manufacturing processes such as fertilizers, insecticides, and phosphate herbicides [7]. Since excess fluoride ingestion would affect human health through dental and skeletal fluorosis, the World Health Organization (WHO) has established a drinking water guideline of 1.5 mg/L for fluoride [23]. Another major anthropogenic source is the semiconductor industry. Hydrofluoric acid (HF) is intensively used in semiconductor process as etching and cleaning agent that generates a large amount of fluoride-containing wastewater [43].

Various technologies have been developed for fluoride removal, including precipitation, fluidized-bed crystallizer, electrocoagulation, adsorption, and ion exchange [23]. Precipitation immobilizes aqueous fluoride as sparingly soluble salts, such as fluorite (CaF_2) and cryolite (Na_3AlF_6) [19,27]. Fluidized-bed crystallizer controls the supersaturation of precipitating species and flow pattern in the reactor to recover the precipitate on the fluidized seeds *via* heterogeneous nucleation and crystal growth [2]. Electrocoagulation applies potential drops across metallic electrodes, preferably iron and aluminum, to facilitate the anodic dissolution of metal ions, namely Fe^{3+} and Al^{3+} species, which precipitates as sweeping flocs under favorable pH conditions and removes aqueous fluoride by adsorption and co-precipitation [24]. Cation exchange resins loaded with Fe^{3+}, La^{3+}, Ce^{4+}, and Zr^{4+} exhibit great affinity and selectivity toward fluoride [33]. Adsorption process has been applied extensively to the removal of fluoride from industrial streams and surface water. There are several types of adsorbents available including aluminum-based (alumina and aluminum hydroxide), carbon-based (activated carbon and biochar), calcium based (calcite and hydroxyapatite) as well as those derived from industrial waste residues (e.g., fly ash, bauxite residue and animal bones) [23,13].

Activated alumina (AA) has been widely applied to the treatment of industrial wastewater and groundwater because of high surface area and high specific adsorption capacity toward fluoride. The uptake of fluoride on AA is highly dependent on solution pH, which governs the speciation of aqueous fluoride and the surface groups of alumina. Hao and Huang [17] pioneered the adsorption of fluoride on alumina quantitatively using the surface complexation model. They proposed that monodentate complex, $\underline{Al}F$, was the major adsorptive species (Eqs. (1) and (2)), accompanied by a bidentate surface complex, $\underline{Al}F_2^-$, (Eq. (3)). Another surface complex, $\underline{Al}OH\text{-}F^-$ (Eq. (4)), was also identified as reversible fluoride surface species by [30] and modeled by Badillo-Almaraz et al., [4]. More complex simulations involving other oxyanions, such as arsenate, selenate, sulfate, bicarbonate, and phosphate have been established also [12,26,37,40].

$$\underline{Al}OH_2^+ + F^- = \underline{Al}F + H_2O \quad \text{at pH} < 6 \tag{1}$$

$$\underline{Al}OH + F^- = \underline{Al}F + OH^- \quad \text{at pH} > 7 \tag{2}$$

$$\underline{Al}OH + 2F^- = \underline{Al}F_2^- + OH^- \tag{3}$$

$$\underline{Al}OH + F^- = \underline{Al}OH\text{ - }F^- \tag{4}$$

Dissolution of Al(III) from AA is a concern during defluorination [14,26]. Alumina has moderate solubility in water that dissolves readily in acidic and alkaline condition. The dissolution of hydrated alumina was found to be related to the density of surface species [29], which was dependent on surface proton concentration. Furthermore, fluoride ion, a Lewis base, tends to complex with Al (III) as fluoroaluminate (AlF_x^{3-x}) and fluorohydroxoaluminate ($AlF_x(OH)_y^{3-x-y}$) in acidic condition, which enhances the solubility of alumina [35]. Meanwhile, the fluoride-occupied surface active sites would accelerate the rate of dissolution [11,35]. The total soluble aluminum leached from AA was 20, 50, and 140 mg-Al/L when the initial fluoride concentration was 100, 500, and 1000 mg-F/L, respectively [12].

Even though the occurrence of Al-F complexes during defluorination by AA has been reported, the adsorption of fluoroaluminate complexes on AA has never been considered. Most literatures simply reported that F^- was a pH-independent species dominant in the solution and responsible for responsible for the fluoride removal as described in Eqs. (1)–(4) [15,16,34]. In the present study, we assessed the role of fluoroaluminate complexes in the adsorption of fluoride on alumina from dilute solutions using pH as a master variable. The dissolution of Al(III) from AA in the presence of fluoride was monitored and calculated by solubility model including fluoroaluminates, which enabled calculate the concentration profile of relevant fluorine species near the alumina surface. The occurrence of fluoroaluminate on the AA surface was supported by XPS. Ultimately, surface complexation model coupling with stability constants of surface Al-F complexes were conducted.

2. Materials and methods

2.1. Activated alumina

Activated alumina (AA) was purchased from China Tatang Corporation, Ltd. Gan Suh, PRC, synthesized by sol-gel method. AA was granulized in spherical shape with diameter between 1 and 3 mm. To remove impurities, 20 g of AA were treated with 50 mL of 0.5 wt % of H_2SO_4 (at a solid to liquid ratio of 400 g/L) for 30 min on a horizontal shaker at 150 rpm. The acid-treated AA was washed by DI thrice using the same solid to liquid ratio and mixing condition. Afterwards, the pretreated AA was dried at 60 °C before use.

2.2. Solubility of activated alumina

The solubility of alumina in solutions was determined as a function of equilibrium pH in the presence of fluoride. A given amount of alumina was added to solution containing different concentrations of NaF with pH value being adjusted to 5, 6, 8, and 9 using 0.1 M of HCl or NaOH. The mixture was mixed thoroughly with a magnetic stir for 2 h. After pH measurement and recording, an aliquot of suspension was sampled and filtered through 0.45-μm mixed cellulose ester membrane (Advantec MFS, Inc. Dublin, CA, USA), to collect the filtrate for the analysis of soluble Al in the solution using ICP-OES (700 Series-710, Agilent, Santa Clara, CA, USA).

2.3. Batch adsorption experiments

Solutions containing 10 to 150 mg-F/L and 10^{-2} M ionic strength were prepared with sodium fluoride (NaF, Honeywell, Charlotte, VA, USA) and sodium perchlorate ($NaClO_4$, Alfa Aesar, Haverhill, MA, USA), respectively, using ultrapure water (resistivity > 18.2 MΩ-cm). $NaClO_4$ was an inert electrolyte often used in adsorption and other chemical reactions experiments [31,41]. Ten g of pretreated AA were mixed with 100 mL of fluoride-containing solution in polyethylene bottle to yield a solid to liquid ratio of 100 g/L. After initial pH adjustment using 1 M of sodium hydroxide (NaOH, Honeywell, Charlotte, VA, USA) and perchloric acid ($HClO_4$, Alfa Aesar, Haverhill, MA, USA), the mixture was mixed on a horizontal shaker at 150 rpm for 2 h at room temperature. After recording the equilibrium pH, filtrate was collected by filtering the supernatant through 0.45-μm syringe filter made of Nylon (Adventec MFS Inc., Dublin, CA, USA). All pH reported in this study were equilibrium values unless otherwise stated.

2.4. Analytical methods

The total fluoride concentration was measured by ion-selective electrode (ISE, ORION-9409BN, Thermo Scientific, Waltham, MA, US). One part of total ionic strength adjusted buffer (TISAB IV, Sigma Aldrich, St. Louis, MO, US) was added to nine parts of sample solution (5.0 < pH < 9.5) during ISE measurement. For samples at pH > 9.5 or pH < 5.0, 4 M of potassium acetate (Sigma Aldrich, St. Louis, MO, US) was added prior to ISE measurement. The pH value was measured by pH meter (FEP-20 FiveEasy-Plus, Mettler Toledo, Columbus, OH USA), which was calibrated weekly. The concentration of aluminum was analyzed by inductively coupled plasma optical emission spectrometer (ICP-OES, 700 Series-710, Agilent). An ion chromatography (ICS-1000, Dionex) was used to analyze sulfate and phosphate. Chromatographic carrier was composed of 0.15 mM Na_2CO_3 and 1.35 mM $NaHCO_3$.

The specific surface area, pore volume and pore size distribution of AA was analyzed by Micromertics ASAP 2020 (Micromertics Instrument Co. Norcross, GA, USA). The specimen was vacuum-dried at 110 °C for 24 h to remove gases. $N_{2(g)}$ adsorption and desorption were conducted at 77 K. The specific surface area and pore volume were calculated according to Brunauer–Emmett–Teller (BET) model and Barrett-Joyner-Halenda (BJH) model, respectively. AA samples used for crystallinity characterization and zeta-potential measurements were first ground with agate mortar and pestle then passed through 150-μm sieve (No. 100). The crystalline phase of AA was characterized by X-ray diffraction (XRD, Bruker D8 Advance, Billerica, MA, USA) with Ni-filtered Cu Kα radiation (λ = 1.5406 Å) operated at a generator voltage of 40 kV and an emission current of 40 mA. The X-ray diffraction patterns were recorded in the 2θ angle range from 10° to 85° with a step size of 0.05° and a scan rate of 2°/min. The zeta-potential of AA suspension (solid to liquid ratio of 0.1 g/L) was measured using a zetasizer (Zetasizer 3000, Malvern, Worcestershire, UK) in 10^{-3} to 10^{-1} M $NaClO_4$ electrolyte. The Al2p and C1s spectra of X-ray photoelectron spectroscopy (XPS) was measured with PHI Quanteral, ULVAC-PHI Inc. (Kanagawa, Japan) with a step size of 0.1 eV under vacuum condition (<1 × 10^{-8} Pa) using an X-ray radiation generated by the excitation of Al-Kα (1486.6 eV) at 15 kV and 10 mA. All the binding energy was referenced to the C 1s signal at 284.8 eV.

3. Theoretical aspects

3.1. Solubility of AA

The solubility of AA was calculated in the absence and the presence of fluoride ion from the total soluble fluoride and aluminum concentration measured. Table 1 summarizes the chemical reactions and corresponding equilibrium constants used in model calculation. The speciation of fluoride species was conducted after solving the fluoride mass balance equation (Eq. (5)) numerically by Matlab 2018a (Mathwork®). The total soluble aluminum, [Al (III)], is therefore obtained by Eq. (6). The activity coefficient of individual ion, γ, was modelled by the Davis equation (Eq. (7)). The subscript of γ in Eqs. (5) and (6) represents the valence of the ion, which varies from −3 to +5.

$$\begin{aligned}[F(-I)] &= [F^-] + [HF] + 2[H_2F_2] + 2\left[HF_2^-\right] + \left[AlF^{2+}\right] + 2\left[AlF_2^+\right] \\ &\quad + 3[AlF_3] + 4\left[AlF_4^-\right] + 5\left[AlF_5^{2-}\right] + 6\left[AlF_6^{3-}\right] \\ &\quad + \left[AlFOH^+\right] + \left[AlF(OH)_2^0\right] + \left[AlF(OH)_3^-\right] + 2\left[AlF_2OH^0\right] \\ &\quad + 2\left[AlF_2OH_2^-\right] + 3[AlF_3OH^-] \\ &= \{F^-\}\left(\begin{array}{l} \frac{1}{\gamma_{-1}} + \frac{\{H^+\}}{K_1} + \frac{2K_3\{H^+\}^2\{F^-\}}{K_2^2} + \frac{2K_4\{H^+\}\{F^-\}}{\gamma_{-1}K_2} \\ + \left\{Al^{3+}\right\}\left(\frac{K_{10}}{\gamma_{+2}} + \frac{2K_{11}\{F^-\}}{\gamma_{+1}} + 3K_{12}\{F^-\}^2 + \frac{4K_{13}\{F^-\}^3}{\gamma_{-1}} + \frac{5K_{14}\{F^-\}^4}{\gamma_{-2}} + \frac{6K_{15}\{F^-\}^5}{\gamma_{-3}}\right) \\ + \frac{K_w\left\{Al^{3+}\right\}}{\{H^+\}}\left(\frac{K_{16}}{\gamma_{+1}} + \frac{K_{17}K_w}{\{H^+\}} + \frac{K_{18}K_w^2}{\gamma_{-1}\{H^+\}^2} + 2K_{19}\{F^-\} + \frac{2K_{20}K_w\{F^-\}}{\gamma_{-1}\{H^+\}} + \frac{3K_{21}\{F^-\}^2}{\gamma_{-1}}\right) \end{array}\right) \end{aligned} \tag{5}$$

$$\begin{aligned}[Al(III)] &= \left[Al^{3+}\right] + \left[AlOH^{2+}\right] + \left[Al(OH)_2^+\right] + \left[Al(OH)_3\right] + \left[Al(OH)_4^-\right] \\ &\quad + 3\left[Al_3(OH)_4^{5+}\right] + \left[AlF^{2+}\right] + \left[AlF_2^+\right] + [AlF_3] + \left[AlF_4^-\right] + \left[AlF_5^{2-}\right] \\ &\quad + \left[AlF_6^{3-}\right] + \left[AlFOH^+\right] + \left[AlF(OH)_2^0\right] + \left[AlF(OH)_3^-\right] + \left[AlF_2OH^0\right] \\ &\quad + \left[AlF_2OH_2^-\right] + [AlF_3OH^-] \\ &= \left\{Al^{3+}\right\}\left(\begin{array}{l} \frac{1}{\gamma_{+3}} + \frac{K_w}{\{H^+\}}\left(\frac{K_5}{\gamma_{+2}} + \frac{K_6K_w}{\gamma_{+1}\{H^+\}} + \frac{K_7K_w^2}{\{H^+\}^2} + \frac{K_8K_w^3}{\gamma_{-1}\{H^+\}^3} + \frac{3K_9K_w^3\left\{Al^{3+}\right\}^2}{\gamma_{+5}\{H^+\}^3}\right) \\ + \{F^-\}\left(\frac{K_{10}}{\gamma_{+2}} + \frac{2K_{11}\{F^-\}}{\gamma_{+1}} + 3K_{12}\{F^-\}^2 + \frac{4K_{13}\{F^-\}^3}{\gamma_{-1}} + \frac{5K_{14}\{F^-\}^4}{\gamma_{-2}} + \frac{6K_{15}\{F^-\}^5}{\gamma_{-3}}\right) \\ + \frac{K_w\{F^-\}}{\{H^+\}}\left(\frac{K_{16}}{\gamma_{+1}} + \frac{K_{17}K_w}{\{H^+\}} + \frac{K_{18}K_w^2}{\gamma_{-1}\{H^+\}^2} + 2K_{19}\{F^-\} + \frac{2K_{20}K_w\{F^-\}}{\gamma_{-1}\{H^+\}} + \frac{3K_{21}\{F^-\}^2}{\gamma_{-1}}\right) \end{array}\right) \end{aligned} \tag{6}$$

$$\log\gamma_i = -0.5 \times z_i^2 \times \left(\frac{\sqrt{I}}{1+\sqrt{I}} - 0.2I\right) \tag{7}$$

where K_w is the ionic product of water (10^{-14}); z_i stands for the valence of ith species; I represents the ionic strength, which is equal to $0.5 \times \sum c_i z_i^2$. Table 1 lists the equilibrium constants of relevant equilibrium equations.

3.2. Surface acidity and complexation model

The surface of hydrous alumina was first treated as amphoteric species by [20], (Eqs. (8) and (9)).

$$\underline{Al}OH_2^+ = \underline{Al}OH + H^+; K_{a1}^{int} = \frac{\{\underline{Al}OH\}\{H^+\}_s}{\{\underline{Al}OH_2^+\}} \tag{8}$$

$$\underline{Al}OH = \underline{Al}O^- + H^+; K_{a2}^{int} = \frac{\{\underline{Al}O^-\}\{H^+\}_s}{\{\underline{Al}OH\}} \tag{9}$$

Table 1
Chemical reactions and the corresponding equilibrium constants considered in $Al_2O_{3(s)}/F^-$ system.[24–26]

No	Reaction	logK	No	Reaction	logK
1	$Al_2O_{3(s)} + 6H^+ = 2Al^{3+} + 3H_2O$	17.87	10	$Al^{3+} + F^- = AlF^{2+}$	7.0
2	$HF = H^+ + F^-$	−3.2	11	$Al^{3+} + 2F^- = AlF_2^+$	12.3
3	$2HF = H_2F_2$	0.4	12	$Al^{3+} + 3F^- = AlF_3^0$	17.0
4	$HF + F^- = HF_2^-$	−0.6	13	$Al^{3+} + 4F^- = AlF_4^-$	19.7
5	$Al^{3+} + OH^- = AlOH^{2+}$	9.0	14	$Al^{3+} + 5F^- = AlF_5^{2-}$	20.8
6	$Al^{3+} + 2OH^- = Al(OH)_2^+$	18.7	15	$Al^{3+} + 6F^- = AlF_6^{3-}$	20.5
7	$Al^{3+} + 3OH^- = Al(OH)_3$	27.0	16	$Al^{3+} + F^- + OH^- = AlFOH^+$	15.4
8	$Al^{3+} + 4OH^- = Al(OH)_4^-$	33.0	17	$Al^{3+} + F^- + 2OH^- = AlF(OH)_2$	23.1
9	$3Al^{3+} + 4OH^- = Al_3(OH)_4^{5+}$	42.1	18	$Al^{3+} + F^- + 3OH^- = AlF(OH)_3^-$	30.1
			19	$Al^{3+} + 2F^- + OH^- = AlF_2OH$	20.1
			20	$Al^{3+} + 2F^- + 2OH^- = AlF_2(OH)_2^-$	27.2
			21	$Al^{3+} + 3F^- + OH^- = AlF_3OH^-$	23.6

where $\underline{Al}OH_2^+$, $\underline{Al}OH$ and $\underline{Al}O^-$ are positively charged, neutral, and negatively charged surface hydroxo sites. The intrinsic surface acidity constants, K_{a1}^{int} and K_{a2}^{int}, describe the conjugated pairs of surface Bronsted acid groups, $\underline{Al}OH_2^+/\underline{Al}OH$ and $\underline{Al}OH/\underline{Al}O^-$, respectively, as a function of surface proton concentration, $\{H^+\}_s$. The parameters of surface acidity, including total site, K_{a1}^{int}, and K_{a2}^{int} were calculated from zeta-potential measurement of AA according to the classic Gouy-Chapman double layer theory under the assumption that surface potential was independent of ionic strength. Detailed calculation of surface acidity is presented in Supplementary Information (S1).

We used surface complexation model to describe the interaction between surface sites and fluorinated species, namely, free fluoride ion and fluoroaluminate complexes, as shown in Eqs. (10)–(13). Eq. (14) is the Boltzmann distribution equation expressing the relationship between surface and bulk concentration of the *i*th ionic species [21].

$$\underline{Al}OH + AlF^{2+} = \underline{Al}OH\text{ - }FAl^{2+}, K_{s1} = \frac{\left\{\underline{Al}OH\text{ - }FAl^{2+}\right\}}{\{\underline{Al}OH\}\left\{AlF^{2+}\right\}_s} \tag{10}$$

$$\underline{Al}OH + AlF_2^+ = \underline{Al}OH\text{ - }F_2Al^+, K_{s2} = \frac{\{\underline{Al}OH\text{ - }F_2Al^+\}}{\{\underline{Al}OH\}\{AlF_2^+\}_s} \tag{11}$$

$$\underline{Al}OH_2^+ + F^- = \underline{Al}OH_2^+\text{ - }F^-, K_{s3} = \frac{\{\underline{Al}OH_2^+\text{ - }F^-\}}{\{\underline{Al}OH\}\{F^-\}_s} \tag{12}$$

$$\underline{Al}OH + F^- = \underline{Al}OH\text{ - }F^-, K_{s4} = \frac{\{\underline{Al}OH\text{ - }F^-\}}{\{\underline{Al}OH\}\{F^-\}_s} \tag{13}$$

$$\{C_i\}_s = [C_i] \times \exp\left(\frac{-z_i F\psi_0}{RT}\right) \tag{14}$$

where $\{C_i\}_s$ and $[C_i]$ are surface and bulk concentrations (M), z_i is the valance of the *i*th species, ψ_0 is the surface potential (V), R is the ideal gas constant (8.314 J $K^{-1}mol^{-1}$), F is the Faraday constant (96485 C mol^{-1}), and T is the absolute temperature (K). The surface potential, ψ_0, was calculated according to the Gouy-Chapmann version of electrical double layer (Supplementary Information, Fig. S4).

In the presence of surface complexes of fluoride and fluoroaluminate, the mass balance equation of surface site can be established as Eq. (15).

$$\begin{aligned}\{\underline{Al}_T\} &= \{\underline{Al}OH_2^+\} + \{\underline{Al}OH\} + \{\underline{Al}O^-\} \\ &+ \left\{\underline{Al}OH\text{ - }FAl^{2+}\right\} + \{\underline{Al}OH\text{ - }F_2Al^+\} + \{\underline{Al}OH_2^+\text{ - }F^-\} + \{\underline{Al}OH\text{ - }F^-\}\end{aligned} \tag{15}$$

By rearranging Eq. (15) with the stability constants from Eqs. (10)–(13), one has Eq. (16), which gives the adsorption density, Γ, in terms of surface concentration of fluoride and fluoroaluminate species:

$$\begin{aligned}\Gamma &= \left\{\underline{Al}OH\text{ - }FAl^{2+}\right\} + 2\{\underline{Al}OH\text{ - }F_2Al^+\} + \{\underline{Al}OH_2^+\text{ - }F^-\} \\ &\quad + \{\underline{Al}OH\text{ - }F^-\} \\ &= \frac{\{Al\}_T\left[K_{s1}\left\{AlF^{2+}\right\}_s + 2K_{s2}\left\{AlF_2^+\right\}_s + \frac{K_{s3}\{H^+\}_s\{F^-\}_s}{K_{a1}^{int}} + K_{s4}\{F^-\}_s\right]}{\frac{\{H^+\}_s}{K_{a1}^{int}} + 1 + \frac{K_{a2}^{int}}{\{H^+\}_s} + K_{s1}\left\{AlF^{2+}\right\}_s + K_{s2}\left\{AlF_2^+\right\}_s + \frac{K_{s3}\{H^+\}_s\{F^-\}_s}{K_{a1}^{int}} + K_{s4}\{F^-\}_s}\end{aligned} \tag{16}$$

The stability constants were calculated using Matlab 2018a (Mathwork®). The adsorption density (Γ_{cal}) was first calculated based on various stability constants ($0.1 \le \log K_{si} \le 10$, $i = 1 \sim 4$). The deviation between the measured (Γ_{obs}) and calculated Γ_{cal} adsorption density was evaluated by chi-square, χ^2, [22]. The stability constants yielding the lowest χ^2 then were established:

$$\chi^2 = \frac{(\Gamma_{obs} - \Gamma_{cal})^2}{\Gamma_{cal}} \tag{17}$$

4. Results and discussion

4.1. Characterization of activated alumina

Fig. S5 shows that γ-Al_2O_3 (JCPDS 10-0425) was the major crystalline phase based on its crystalline phases (3 1 1), (4 4 0), and (4 0 0) at 2θ of 36.2°, 46.1° and 66.9°, respectively. According to the Debye-Scherrer equation [42], the grain size of γ-Al_2O_3 determined was 9.9 nm, which was the averaged value calculated from phases (4 4 0) and (4 0 0). The small crystallite size contributed to the high specific surface area of *ca.* 312 m^2/g. Pore size distribution (Fig. S6) confirmed the presence of pores in the range of mesopore (2–30 nm) with a marked distribution at 4 nm. The total pore volume was estimated at 0.45 cm^3/g according to the BJH model.

Fig. 1 presents the zeta-potentials of AA in solutions at five ionic strengths, 10^{-3} to 10^{-1} M $NaClO_4$. Intersect of five curves suggests that the point of zero charge, pH_{pzc}, was located at 8.5 where the proton-derived surface charge was null. However, an intrinsic positive surface charge that contributes a zeta-potential of 8.8 mV at pH_{pzc} was spotted, which may be contributed by permanent structural charge or specific adsorption of sodium ion in the Stern layer [8]. Table S1 summarizes the position of shear plane derived from linearized Gouy-Chapman equation. The distance of shear plane from the surface were between 4 and 7 Å, which was within the reported range [9]. As shown in Eq. (18), the surface charge density of hydrous surface may come from the structural surface charge (usually caused by isomorphic substitution), specific adsorption of electrolyte in the Stern layer, and surface charge subject to protonation and deprotonation, i.e.,

$$\sigma_T = \sigma_0 + \sigma_S + \sigma_H \tag{18}$$

where σ_T, σ_0, σ_S, and σ_H are total, structural, Stern layer, and net proton surface charge density, respectively. σ_S equals to the sum of inner-sphere complex (σ_{IS}) and outer sphere complex (σ_{OS}) surface charge. With known d, double layer thickness, the zeta-potential at pH_{pzc}, 8.8 mV can be used to calculate the sum of σ_0 and σ_S using Eqs. (S1b) and (S2b) under various ionic strength, as summarized in Table 2. In that case, the net proton surface charge density, σ_H, can be isolated for surface acidity calculation (Section S1 in Supporting

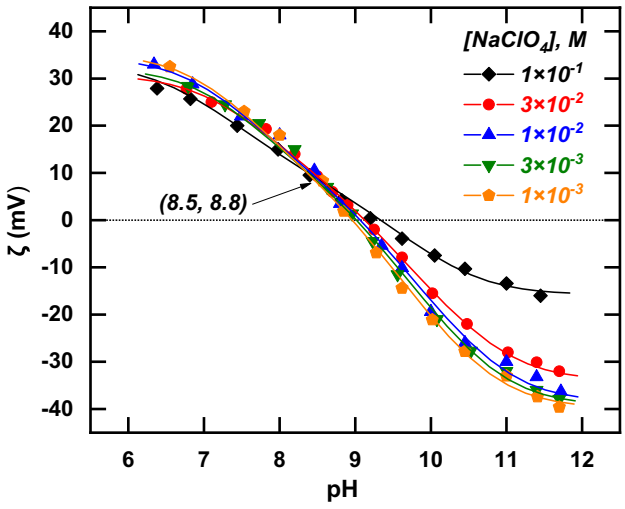

Fig. 1. Zeta potential of activated alumina in $NaClO_4$ electrolyte. (Lines are fitted results).

Table 2
Surface acidity parameters of activated alumina under various ionic strength.

$NaClO_4$ (M)	1×10^{-3}	3×10^{-3}	1×10^{-2}	3×10^{-2}	1×10^{-1}
$\sigma_0 + \sigma_S$ (C m^{-2})	6.44×10^{-4}	1.16×10^{-3}	2.29×10^{-3}	4.49×10^{-3}	1.05×10^{-2}
pK_1^{int}	8.01	8.04	8.02	8.18	7.90
pK_2^{int}	9.52	9.60	9.65	9.63	9.54
$\{\underline{Al}_T^+\}$(C m^{-2})	2.28×10^{-3}	3.61×10^{-3}	8.04×10^{-3}	1.36×10^{-2}	3.91×10^{-2}
$\{\underline{Al}_T^-\}$(C m^{-2})	4.00×10^{-3}	7.20×10^{-3}	1.41×10^{-2}	2.49×10^{-2}	3.08×10^{-2}
Average $\{\underline{Al}_T\}$ (C m^{-2})	3.14×10^{-3}	5.41×10^{-3}	1.11×10^{-2}	1.93×10^{-2}	3.50×10^{-2}

Information). Table 2 summarizes the surface acidity parameters, based on data present in Fig. 1, used in model simulation. The observed zeta-potential data in Fig. 1 closely followed the fitted line, indicating that Gouy-Chapman theory and surface acidity theory could describe the surface charge of AA well. The intrinsic constants, K_{a1}^{int} and K_{a2}^{int}, were a function of ionic strength as expected. At ionic strength of 1×10^{-2} M, the intrinsic acidity constants, K_{a1}^{int} andK_{a2}^{int}, were $10^{-8.03}$ and $10^{-9.59}$, respectively. The values were in agreement with previously reported: $10^{-7.70}$ and $10^{-9.30}$ by Huang and Stumm [20], $10^{-8.18}$ and $10^{-9.48}$ by Yang et al. [45].

4.2. Dissolution of activated alumina in the presence of fluoride

Aluminum ion is a strong Lewis acid and can be easily bound by electron-rich molecules, such as hydroxyl ion and fluoride ion [32]. Fig. 2a shows that alumina has low solubility ([Al(III)] < 10^{-5} M) in

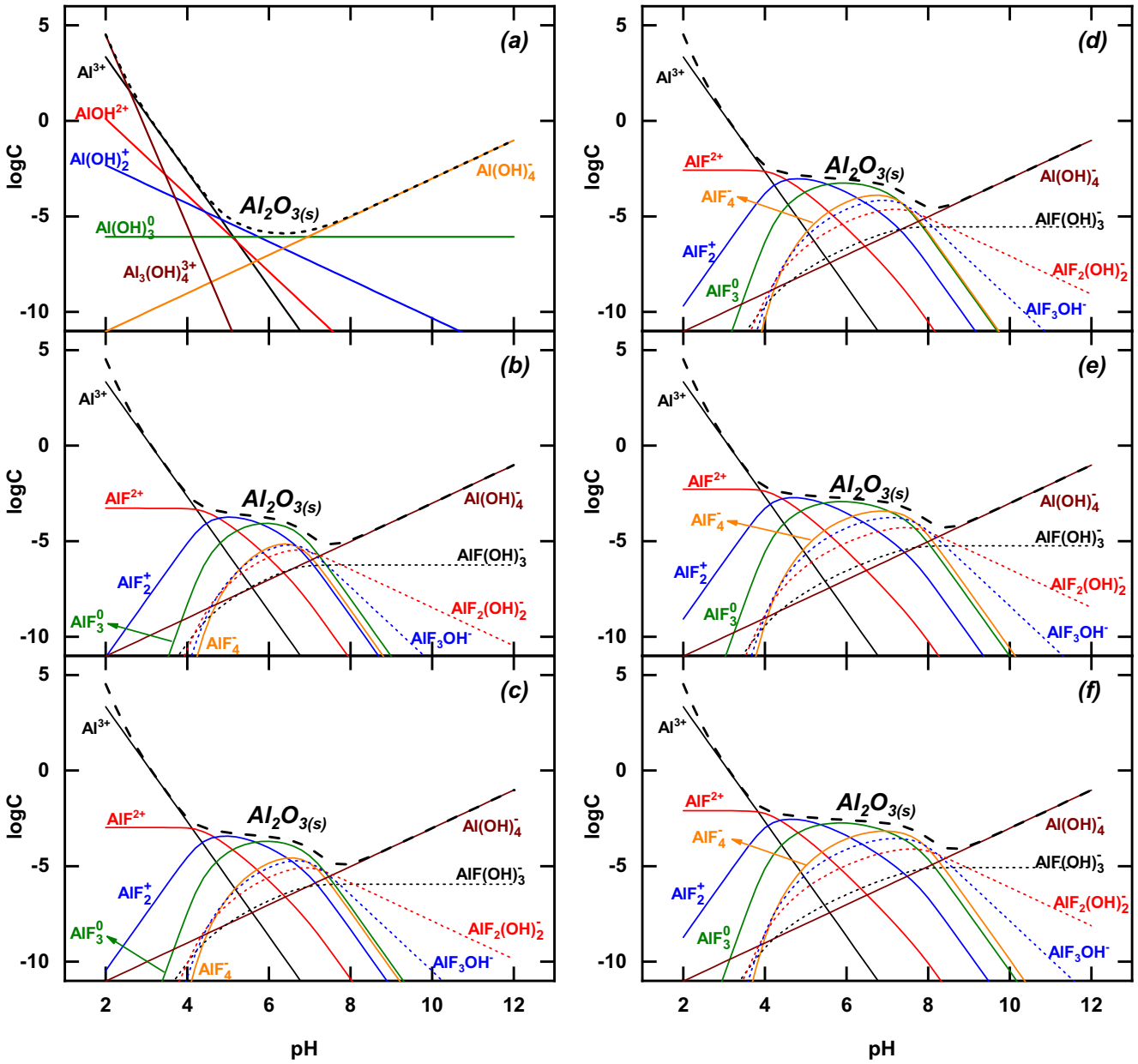

Fig. 2. Solubility curves of $Al_2O_{3(s)}$ in the absence of fluoride ion (a) and in the presence of (b) 10, (c) 20, (d) 50, (e) 100 and (f) 150 mg-F/L. (Ionic strength = 10^{-2} M).

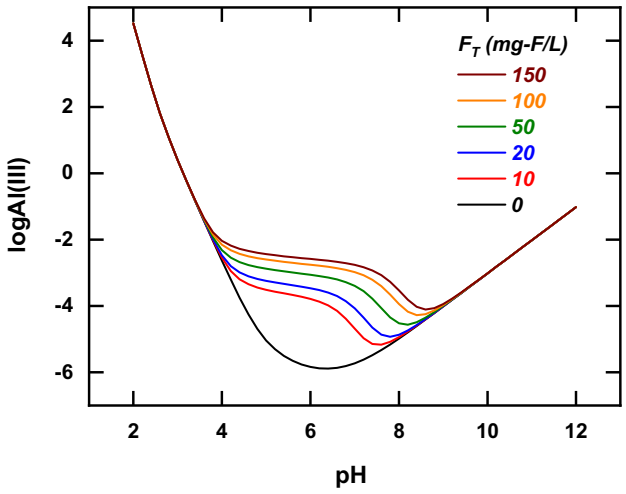

Fig. 3. Effects of total fluoride concentration on solubility $Al_2O_{3(s)}$. (Ionic strength = 10^{-2} M).

the pH range of 5 to 9 and the absence of fluoride; Al^{3+} and $Al(OH)_4^-$ are the solubility-determining species at pH < 5 and >9, respectively. Fig. 2b-f depicts the solubility of alumina in the presence of fluoride ranging from 10 to 150 mg-F/L. Fluoroaluminate complexes (AlF_x^{3-x}) predominate at pH < 7, even in the presence of only 10 mg-F/L, greatly elevating the solubility of alumina by one hundred times at neutral condition. Fluorohydroxoaluminates ($AlF_x(OH)_y^{3-x-y}$) form at higher pH, where hydroxyl anion is sufficient to compete for the Lewis acid site (i.e., surface aluminum ion) with fluoride ligand, and therefore enhances the solubility of alumina at pH > 9. The increase in total fluoride concentration promotes the formation of fluoro(hydroxo)aluminate, especially highly fluorinated complexes at neutral pH, e.g. AlF_3, AlF_4^-, $AlF_2(OH)_2^-$ and AlF_3OH^-. Results in Fig. 3 shows that fluoride ion significantly enhances the solubility of alumina over a wide pH range of 4–9.

One may concern the possible influence of calcium ion, Ca^{2+}, a major cation of natural water and many industrial waste streams, on the solubility of $Al_2O_3(s)$ in fluoride containing solution due to $CaF_2(s)$ precipitation. As shown in Figs. S7 and S8, when $Al_2O_3(s)$ is in equilibrium with 10 mg-F/L and 15 mg-Ca/L, $CaF_2(s)$ starts to precipitate at pH > 6.9 that rendered slight decrease in total fluoride concentration and the solubility of $Al_2O_3(s)$. The degree of interference by $CaF_2(s)$ precipitation on alumina dissolution intensifies as the background fluoride concentration increases. Total soluble fluoride concentration was controlled by the solubility of $CaF_2(s)$ at pH > 6.9 under which condition the formation of fluoroaluminates was greatly suppressed and so was the solubility of AA.

In order to validate the model prediction of dissolution of alumina in the presence of fluoride, the observed and calculated Al (III) at the end of defluorination were compared. Fig. 4 shows that by applying the measured [F(-I)] and pH into Eqs. (5)–(7), the solubility model predicted the concentration of Al(III) well. Notably, the deviations increased as initial fluoride decreased. It is known that the dissolution of Al_2O_3 is governed by proton-promoted dissolution from $\underline{Al}OH_2^+$, OH^--promoted dissolution from AlO^-, and ligand-promoted dissolution from $\underline{Al}F_x$. The dissolution rate of alumina was reported to be accelerated by fluoride at concentration greater than 10^{-6} M [49]. In other words, the dissolution of alumina should be faster in more concentrated fluoride solution since the population of fluoride-bound surface species increased. The observed Al(III) approached the theoretical values under high initial fluoride concentrations due to significant ligand-promoted dissolution.

4.3. Adsorptive removal of fluoride by activated alumina

Fig. 5 shows the fluoride adsorption density of AA with various initial fluoride concentrations as a function of equilibrium pH.

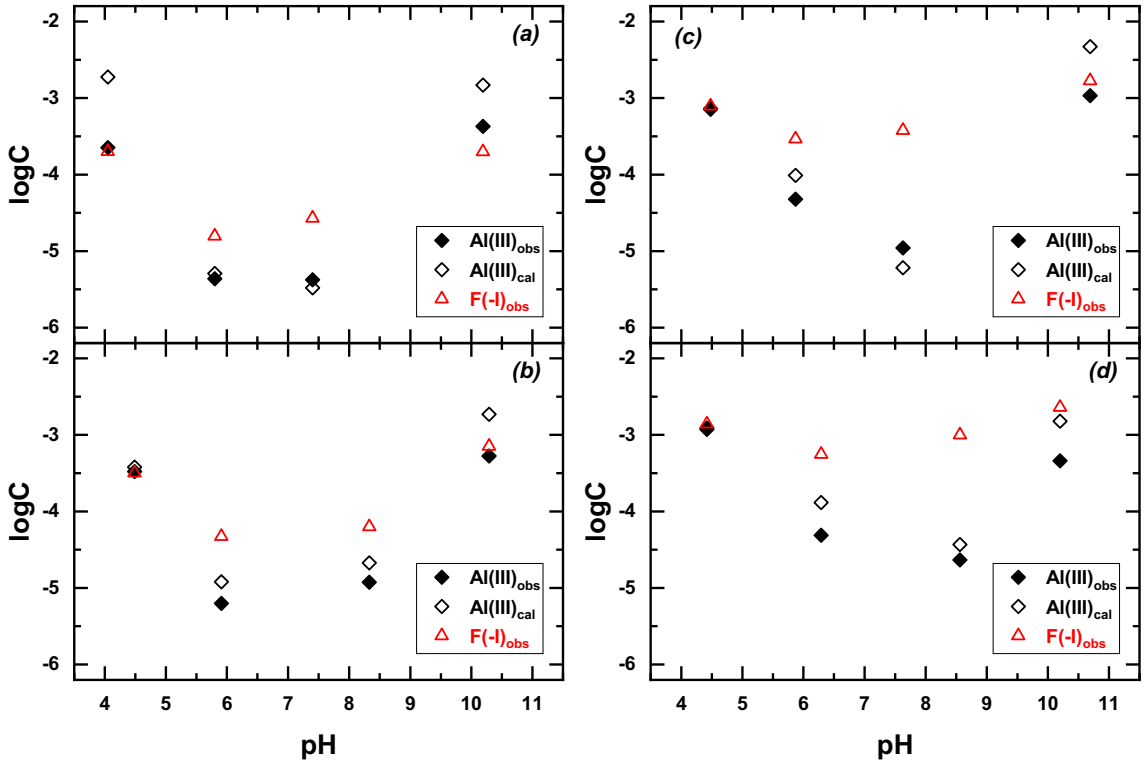

Fig. 4. Concentration of calculated Al(III), observed Al(III) and F(-I) at the end of adsorption process using AA with initial fluoride level of (a) 20, (b) 50, (c) 100 and (d) 150 mg-F/L. ([$NaClO_4$] = 10^{-2} M, S/L = 100 g/L, equilibrium time = 2 h.)

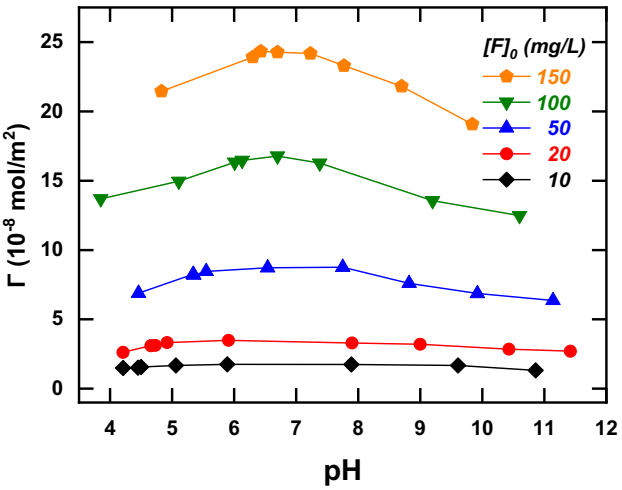

Fig. 5. Adsorption density as a function of pH_e with various initial fluoride concentration. ($[NaClO_4] = 10^{-2}$ M, S/L = 100 g/L, equilibrium time = 2 h.)

Noted that the adsorption density was corrected for the amount of alumina loss due to dissolution (S3, Supporting Information). The adsorption density showed positive correlation with initial fluoride concentration because of increase in the fraction of adsorbed active sites with increase in residual fluoride concentration [39]. The maximal adsorption density was at pH 6.5, mainly contributed by the surface complexes of $\underline{Al}OH\text{-}F_2Al^+$, $\underline{Al}OH_2^+\text{-}F^-$, and $\underline{Al}OH\text{-}F^-$ (discussed later). Fig. 6 presents the surface and bulk concentration of fluoride and fluoroaluminates as a function of pH, calculated from the observed total fluoride concentration. In the bulk solution, F^- was the dominant species at pH > 5.5, while AlF^{2+}, AlF_2^+ and AlF_3 prevailed at pH < 5.5. When the surface potential was considered (Eq. (14)), the surface concentration of positively charged fluoroaluminates, AlF^{2+} and AlF_2^+, were around 40-fold and 7-fold, respectively, lower than the bulk concentration due to electrostatic repulsive force exerted by the protonated active sites ($\underline{Al}OH_2^+$). On the other hand, the surface concentration of F^- was greater than the bulk concentration at pH < pH_{pzc} but lower at pH > pH_{pzc}. The concentration of AlF_3 as a neutral species was unaffected by the charged surface. The profile of surface concentration revealed that fluoroaluminate complexes prevailed over F^- in acidic condition

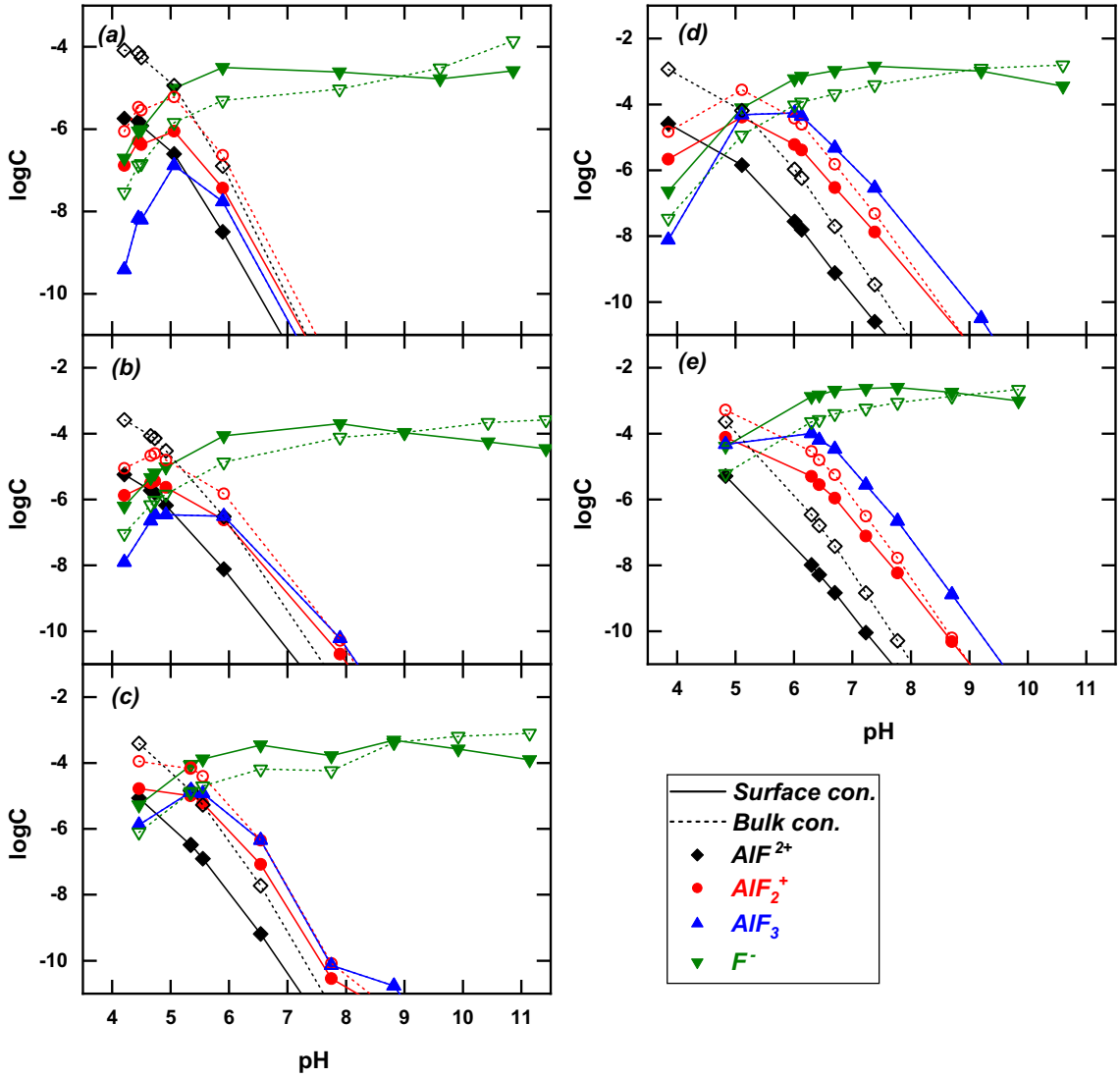

Fig. 6. Surface and bulk concentration of fluoride and fluoroaluminate as a function of bulk pH with initial fluoride concentration of (a) 10, (b) 20, (c) 50, (d) 100 and (e) 150 mg-F/L. ($[NaClO_4] = 10^{-2}$ M, S/L = 100 g/L, equilibrium time = 2 h.).

that the adsorption of species such as $\underline{Al}OH\text{-}FAl^{2+}$, $\underline{Al}OH\text{-}F_2Al^{+}$, and $\underline{Al}OH\text{-}F_3Al$ on AA could not be oversighted.

Fig. S9 shows the zeta-potential of AA in the presence of fluoride (5–100 mg-F/L). Results indicated that pH_{pzc} was decreased slightly from 8.4 to 8.0 then to 7.1 in the presence of 50 mg-F/L and 100 mg-F/L, respectively, with respect to that in background electrolyte of 10^{-2} M $NaClO_4$. Obviously, the interaction between fluorinated cations and neutral surface hydoxo (AlOH) species with the formation of surface complexes, namely, $\underline{Al}OH\text{-}FAl^{2+}$ and $\underline{Al}OH\text{-}F_2Al^{+}$, rendered the surface charge positive (cf, pH < 5 region). Further increase in total fluoride concentration and thus adsorption of F^- on positive ($\underline{Al}OH_2^+$) and neutral ($\underline{Al}OH$) surface sites rendered the surface charge negative. Results clearly showed surface charge reversal, which implied specific adsorption of fluoroaluminates and fluoride ions.

Fig. S10 gives the fluoride adsorption isotherm at pH 6. The adsorption isotherm was fitted by Langmuir and Fruendlich models (Fig. S10). Table S2 lists the fitted model parameters. Both models exhibited high R^2 value of >0.98. Question rises on the effect of major anions on fluoride adsorption on AA. The adsorption selectivity of AA between F^-, $H_2PO_4^-$ and SO_4^{2-} was examined based on selectivity coefficient, *k*, which is the ratio of distribution coefficients, K_d [36].

$$K_d = \frac{\Gamma}{C_e} \tag{19}$$

$$k = \frac{K_d(F^-)}{K_d(X)} \tag{20}$$

where Γ is adsorption density (mol/m^2), C_e is equilibrium concentration (mol/L) and *X* represents the competing anion, e.g., SO_4^{2-} and $H_2PO_4^-$. Table 3 gives the adsorption density and distribution coefficient of the anions and their selectivity coefficient with respect to fluoride. The adsorptive affinity toward AA surface followed the order: $F^- > H_2PO_4^- > SO_4^{2-}$ based on K_d in single anion system. In the binary system of F^- and SO_4^{2-}, the great selectivity coefficient of SO_4^{2-} (~250) suggested that sulfate ion could barely compete with fluorinate species for active sites. Tor et al. [38] reported that sulfate tended to form outer-sphere complex *via* electrostatic attraction and resulted in limited active sites on the surface. Note that bicarbonate is a weaker ligand than sulfate toward most Lewis acid. Therefore, the affinity of HCO_3^- toward AA, though not determined, would be expectedly weaker than SO_4^{2-}. Tang et al. [37] reported that HCO_3^- and SO_4^{2-} were not as competitive as fluoride in adsorption on AA. On the contrary, $H_2PO_4^-$ showed comparable adsorption affinity with respect to fluorinated species, resulting in a selectivity coefficient of 1.3 in binary system, which was consistent with the work of Mouelhi et al. [34] and Tang et al. [37]. Inner-sphere complexation has been reported to be the main mechanism for phosphate adsorption on alumina, which occupies the active sites for further adsorption of fluorinated species, while the selectivity remained unchanged in ternary system [48].

4.4. Adsorption of major fluoride species on AA

As discussed above, Fig. 6 showed that fluoroaluminate complexes were the dominating species at pH < 6. At pH > 7, the dominating species was fluoride ion. The decrease in pH_{pzc} in the presence of fluoride also suggested the possible adsorption of cationic fluoroalumiantes on AA surface. Therefore, XPS spectra of pristine and fluoride-laden AA in the pH range of 5–9 were acquired to verify the chemical state thereby the possible presence of adsorbed fluoride species on AA surface. Only one peak was observed in pristine AA at 74.2 eV, which was between the Al-O binding energy of aluminum oxide (74.1 eV) and pseudoboehmite (AlOOH), when surveying binding energy spectra of Al 2p (Fig. 7) [25]. Since the pristine AA was acidified and washed prior to surface analysis, some of the surface aluminum oxide could be hydrated to oxyhydroxide. The AA in contact with fluoride containing solutions at pH 5 to 9 exhibited additional peaks at 75.1 to 75.4 eV, respectively. These peaks must be attributed to the presence of Al—F bonds due to the formation of inner-sphere complexes of $\underline{Al}$-F or $\underline{Al}$- fluoroaluminates, e.g., $\underline{Al}OH\text{-}FAl^{2+}$, $\underline{Al}OH\text{-}F_2Al^{+}$ and $\underline{Al}OH\text{-}F_3Al$. Note that previous studies have attributed the increased binding energy to the adsorption of fluoride ion on hydrated alumina surface without clarification [1,40,44,46,47].

Fig. 7 shows that the fraction of Al—F bond on AA surface decreased with pH, from 21.4% at pH 5.0 to 9.9% at pH 9.4, a two-time increase, while the adsorption density remained relatively unchanged in the same pH range of 5 to 9 (215–245 nmol/m^2 at initial fluoride concentration of 150 mg-F/L, Fig. 5). Results suggested that the mechanism of fluoride adsorption on AA in acidic condition was different from that in alkaline solution as seen from the decrease in Al—F bond energy intensity from XPS survey. In alkaline condition, the fluoride ion was immobilized on AA through inner-sphere complexation ($\underline{Al}$-F) and hydrogen bonding ($\underline{Al}OH\text{-}F^-$); the former appeared at the binding energy of 75.4 eV, whereas the latter could not be detected by XPS. On the other hand, in acidic condition, once adsorbed, even by hydrogen bonding, fluoroaluminates were detectable still by XPS,. Therefore, the intensity of Al—F bond at pH 5.0 was much greater than that at pH 9.4 even though the apparent adsorption density was comparable. Transition of the adsorbed fluorinated species from that of flu-

Table 3
Adsorption density, distribution and selectivity coefficient of F^-, SO_4^{2-} and $H_2PO_4^-$ on AA at pH 6.

Adsorption density, nmol/m^2	Singe anion	Binary system		Ternary system
		F^-/SO_4^{2-}	$F^-/H_2PO_4^-$	$F^-/SO_4^{2-}/H_2PO_4^-$
F^-	163	160	148	150
SO_4^{2-}	118	13	–	5
$H_2PO_4^-$	146	–	135	133
Distribution coefficient, μL/m^2	Singe anion	Binary system		Ternary system
		F^-/SO_4^{2-}	$F^-/H_2PO_4^-$	$F^-/SO_4^{2-}/H_2PO_4^-$
$K_d(F^-)$	356	339	175	160
$K_d(SO_4^{2-})$	64	1.3	–	0.5
$K_d(H_2PO_4^-)$	149	–	130	121
Selectivity coefficient	Binary system		Ternary system	
	F^-/SO_4^{2-}	$F^-/H_2PO_4^-$	$F^-/SO_4^{2-}/H_2PO_4^-$	
$k(SO_4^{2-})$	252	–	293	
$k(H_2PO_4^-)$	–	1.3	1.3	

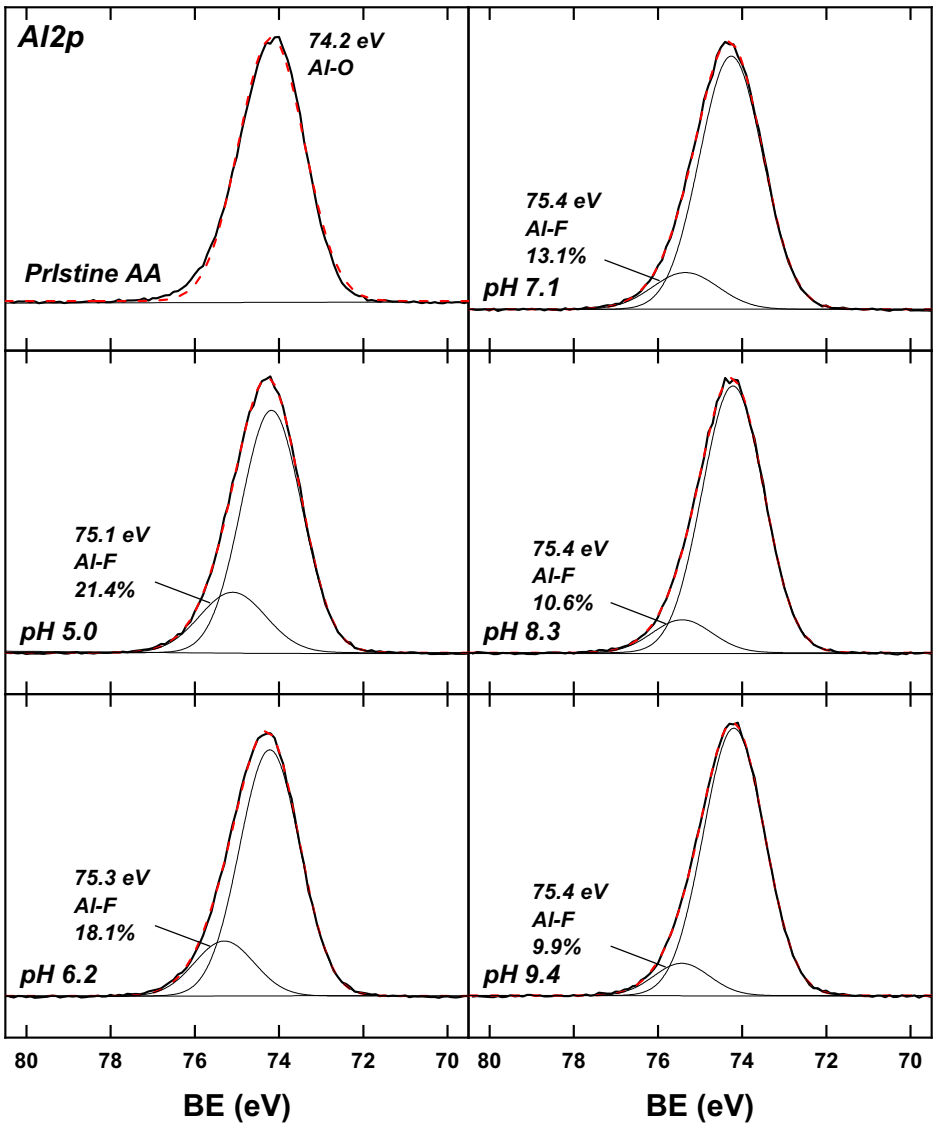

Fig. 7. XPS spectra in Al2p region of pristine AA and fluoride-laden AA at various pH values. ($[F]_0$ = 150 mg-F/L, $[NaClO_4] = 10^{-2}$ M, S/L = 100 g/L, equilibrium time = 2 h).

oroaluminates to fluoride ion as pH increased resulted in a decrease in the fraction of surface Al-F. The Al 2p binding energy increased with the number of fluoride bound to aluminum according to Hess et al., [18], who reported that the Al 2p binding energy of $AlF_2(OH)$, $AlF_{2.3}(OH)_{0.7}{\cdot}H_2O$, β-$AlF_3$ and α-AlF_3 were 76.2, 75.8, 76.9 and 77.1 eV, respectively. Thus, the major adsorbed species on AA in acidic condition are likely to be AlF^{2+} and AlF_2^+.

4.5. Surface complexation model involving fluoroaluminate

The surface complexation model involving Al-F complexes was based on the following interactions between fluoroaluminates, mainly, AlF^{2+} and AlF_2^+, and the neutral surface hydroxo species (≡AlOH) on AA, via hydrogen bonding, with the formation of ≡Al-OH-FAl^{2+} and ≡AlOH-F_2Al^+ surface complexes:

$$\equiv AlOH + AlF^{2+} \rightleftharpoons \equiv AlOH - AlF^{2+}; K_{s1} \quad (21a)$$

$$\equiv AlOH + AlF_2^{+} \rightleftharpoons \equiv AlOH - AlF_2^{+}; K_{s2} \quad (21b)$$

Likewise, F^- would bind with the positively charged hydroxo species, $\equiv AlOH_2^+$, and the neutral surface hydroxo species, ≡AlOH, also via hydrogen bond, to form $\equiv AlOH_2^+$-F^- and ≡AlOH-F^- surface complexes [30]:

$$\equiv AlOH_2^{+} + F^- \rightleftharpoons \equiv AlOH_2^{+} - F^-; K_{s3} \quad (21c)$$

$$\equiv AlOH + F^- \rightleftharpoons \equiv AlOH - F^-; K_{s4} \quad (21d)$$

Stability constants (K_s) of above surface complexes were given in Eqs. (10)–(13). The adsorption data of Fig. 5 were fitted by Eq. (16) with total site density, $\{Al_T\}$, of 7.90×10^{-7} mol/m^2, from

Table 4
Stability constants of fluoroaluminate and fluoride surface complex.

$[F]_0$ (mg-F/L)	$\log K_{s1}$	$\log K_{s2}$	$\log K_{s3}$	$\log K_{s4}$
10	6.9	4.9	3.2	2.8
20	6.7	6.0	2.7	2.2
50	6.7	5.4	2.9	2.4
100	7.2	5.1	2.4	2.3
150	6.9	5.4	2.4	2.1
Average	6.88	5.36	2.72	2.36

$\equiv AlOH + AlF^{2+} \rightleftharpoons \equiv AlOH - AlF^{2+}; K_{s1}$.
$\equiv AlOH + AlF_2^{+} \rightleftharpoons \equiv AlOH - AlF_2^{+}; K_{s2}$.
$\equiv AlOH_2^{+} + F^- \rightleftharpoons \equiv AlOH_2^{+} - F^-; K_{s3}$.
$\equiv AlOH + F^- \rightleftharpoons \equiv AlOH - F^-; K_{s4}$.

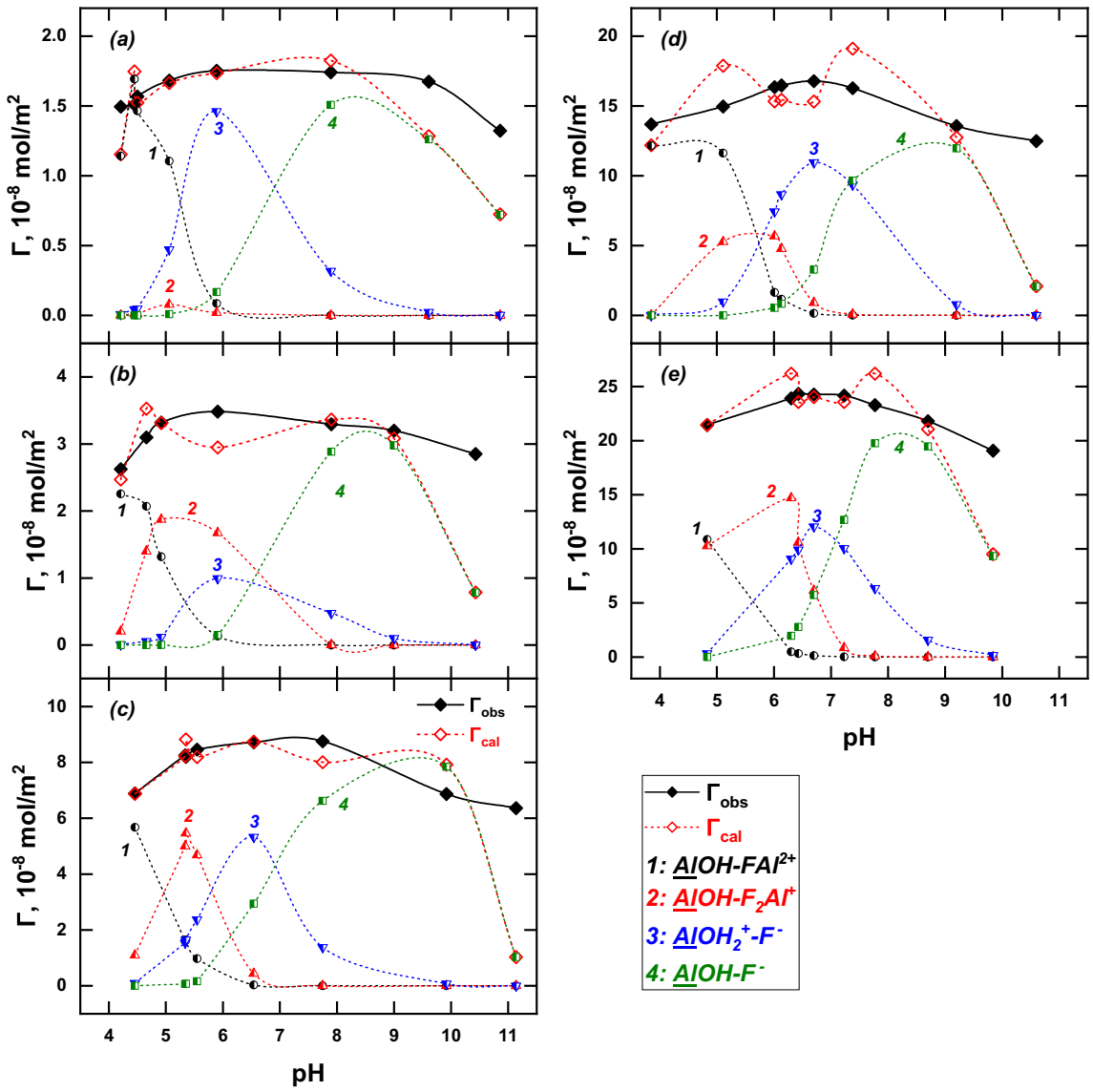

Fig. 8. Fitting of fluoride and fluoroaluminate adsorption on activated alumina with initial fluoride concentration of (a) 10, (b) 20, (c) 50, (d) 100 and (e) 150 mg-F/L. ($[NaClO_4] = 10^{-2}$ M, S/L = 100 g/L, equilibrium time = 2 h).

the Langmuir isotherm model (Table S2). Table 4 summarizes the obtained stability constants. Furthermore, the Gibbs free energy of the surface complexes were estimated using Eq. (21):

$$\Delta G = -2.303RT\log K_s \quad (21)$$

where R is ideal gas constant (8.314 J mol^{-1} K^{-1}) and T is temperature (K). The free energy of adsorption for $\underline{Al}OH\text{-}FAl^{2+}$, $\underline{Al}OH\text{-}F_2Al^{+}$, $\underline{Al}OH_2^{+}\text{-}F^{-}$ and $\underline{Al}OH\text{-}F^{-}$ were −393, −306, −155 and −135 kJ/mol, respectively. The magnitude of ΔG^o strongly suggested hydrogen bonding was involved in the formation of above surface complexes [6].

Fig. 8 depicts the observed and calculated adsorption density, along with the speciation of surface complexes. The results showed that $\underline{Al}OH\text{-}FAl^{2+}$ and $\underline{Al}OH\text{-}F_2Al^{+}$ contributed to the total fluoride adsorption density at pH < 6; the latter species even populated till pH 7 at high initial fluoride concentration. The surface complexes of F^-, i.e. $\underline{Al}OH_2^{+}\text{-}F^{-}$ and $\underline{Al}OH\text{-}F^{-}$, were the major species at pH > 7. Deviations from observed adsorption density in alkaline condition might be attributed to competition for surface sites by sodium ions that blocked sites otherwise were available for fluoride ions [12]. Above findings suggested that free fluoride ion was a major species responsible for adsorption on AA under the pH condition of typical surface water and groundwater. However, the formation of fluoroaluminates such as AlF^{2+}, AlF_2^{+} in acidic pH environment can affect the adsorption of total fluoride. Therefore, the effect of fluoroaluminates on fluoride adsorption on AA must be considered, in addition to free fluoride, in the design of treatment processes for specific industrial wastewaters such as electroplating, semiconductor manufacturing, and metal processing [10,3,5,28].

5. Conclusion

This study revisited the defluorination by activated alumina and verified that fluoroaluminates (AlF_x^{3-x}), originated from the dissolution of activated alumina (AA), were the main adsorbates in acidic condition, whereas the fluoride ion was the sole species adsorbed on AA surface in neutral and alkaline condition. Experimental data and results of solubility calculation revealed that the

solubility of AA in fluoride solution was significantly enhanced owing to the formation of AlF_x^{3-x} at pH < 7 and $AlF_x(OH)_y^{3-x-y}$ at pH > 7. At pH < 5, the dominant fluoroaluminate species were AlF^{2+}, AlF_2^+ and AlF_3. The fraction of Al-F, based on Al2p binding energy, decreased from 21.4 to 9.9% as pH increased from 5.0 to pH 9.4, which indicated the transition of the adsorbed species from that of fluoroaluminates to free fluoride ions.pristine Therefore, a surface complexation model including surface complexes of AlF^{2+}, AlF_2^+ and F^- was derived to fit the adsorption edge with initial fluoride concentration of 10 to 150 mg-F/L. Stability constant of the four fluorinated surface complexes, $\underline{Al}OH\text{-}FAl^{2+}$, $\underline{Al}OH\text{-}F_2Al^+$, $\underline{Al}OH_2^+\text{-}F^-$, and $\underline{Al}OH\text{-}F^-$, were $10^{6.88}$, $10^{5.36}$, $10^{2.72}$, and $10^{2.36}$, respectively. Magnitude of stability constants implied hydrogen bonding was involved with the attachment of fluroaluminates and free fluoride ions.

Declaration of Competing Interest

The authors declare that they have no known competing financial interests or personal relationships that could have appeared to influence the work reported in this paper.

Acknowledgement

This work was supported by the ROC Ministry of Science and Technology through grands MOST 105-2221-E-009-006-MY3 and MOST 108-2622-8-009-002-TE5. Additional support was provided by US National Science Foundation, through grand US NSF IOA (1632899).

Appendix A. Supplementary material

Supplementary data to this article can be found online at https://doi.org/10.1016/j.jcis.2019.10.085.

References

[1] R.C. Arthur, H. Sasamoto, M. Shibata, M. Yui, A. Neyama, Development of thermodynamic databases for geochemical calculations, Japan Nucl. Cycle Dev. Inst. (1999).
[2] R. Aldaco, A. Garea, A. Irabien, Calcium fluoride recovery from fluoride wastewater in a fluidized bed reactor, Water Res. 41 (2007) 810–818.
[3] S. Aoudj, A. Khelifa, N. Drouiche, M. Hecini, Removal of fluoride and turbidity from semiconductor industry wastewater by combined coagulation and electroflotation, Desalinat. Water Treat. 57 (2016) 18398–18405.
[4] V.E. Badillo-Almaraz, M.J. Solache-Ríos, V. Badillo-Almaraz, A. Zarate-Morales, A. Flores-Moreno, Radiotracer techniques (^{18}F) and modeling of fluoride sorption on alumina, J. Fluor. Chem. 199 (2017) 113–118.
[5] M. Chaudhary, A. Maiti, Defluoridation by highly efficient calcium hydroxide nanorods from synthetic and industrial wastewater, Colloids Surf. Physicochem. Eng. Asp. 561 (2019) 79–88.
[6] M.O. Corapcioglu, C.P. Huang, The adsorption of heavy metals onto hydrous activated carbon, Water Res. 21 (1987) 1031–1044.
[7] P.S. Datta, D.L. Deb, S.K. Tyagi, Stable isotope (^{18}O) investigations on the processes controlling fluoride contamination of groundwater, J. Contam. Hydrol. 24 (1996) 85–96.
[8] W.B.S. de Lint, N.E. Benes, J. Lyklema, H.J.M. Bouwmeester, A.J. van der Linde, M. Wessling, Ion adsorption parameters determined from zeta potential and titration data for a γ-alumina nanofiltration membrane, Langmuir 19 (2003) 5861–5868.
[9] W. Ding, X. Liu, L. Song, Q. Li, Q. Zhu, H. Zhu, F. Hu, Y. Luo, L. Zhu, H. Li, An approach to estimate the position of the shear plane for colloidal particles in an electrophoresis experiment, Surf. Sci. 632 (2015) 50–59.
[10] A. Ezzeddine, A. Bedoui, A. Hannachi, N. Bensalah, Removal of fluoride from aluminum fluoride manufacturing wastewater by precipitation and adsorption processes, Desalinat. Water Treat. 54 (2015) 2280–2292.
[11] H. Farrah, J. Slavek, W. Pickering, Fluoride interactions with hydrous aluminum oxides and alumina, Soil Res. 25 (1987) 55.
[12] H.R. Fletcher, D.W. Smith, P. Pivonka, Modeling the sorption of fluoride onto alumina, J. Environ. Eng. 132 (2006) 229–246.
[13] J. Ge, S. Yoon, N. Choi, Application of fly ash as an adsorbent for removal of air and water pollutants, Appl. Sci. 8 (2018) 1116.
[14] S. George, P. Pandit, A.B. Gupta, Residual aluminium in water defluoridated using activated alumina adsorption – Modeling and simulation studies, Water Res. 44 (2010) 3055–3064.
[15] W.-X. Gong, J.-H. Qu, R.-P. Liu, H.-C. Lan, Adsorption of fluoride onto different types of aluminas, Chem. Eng. J. 189–190 (2012) 126–133.
[16] A. Goswami, M.K. Purkait, The defluoridation of water by acidic alumina, Chem. Eng. Res. Des. 90 (2012) 2316–2324.
[17] O.J. Hao, C.P. Huang, Adsorption characteristics of fluoride onto hydrous alumina, J. Environ. Eng. 112 (1986) 1054–1069.
[18] A. Hess, E. Kemnitz, A. Lippitz, W.E.S. Unger, D.H. Menz, ESCA, XRD, and IR characterization of aluminum oxide, hydroxyfluoride, and fluoride surfaces in correlation with their catalytic activity in heterogeneous halogen exchange reactions, J. Catal. 148 (1994) 270–280.
[19] C.J. Huang, J.C. Liu, Precipitate flotation of fluoride-containing wastewater from a semiconductor manufacturer, Water Res. 33 (1999) 3403–3412.
[20] C.-P. Huang, W. Stumm, Specific adsorption of cations on hydrous γ-Al_2O_3, J. Colloid Interface Sci. 43 (1973) 409–420.
[21] C.P. Huang, J. Wang, Specific chemical interactions between metal ions and biological solids exemplified by sludge particulates, Bioresour. Technol. 160 (2014) 32–42.
[22] M.H. Isa, E.H. Ezechi, Z. Ahmed, S.F. Magram, S.R.M. Kutty, Boron removal by electrocoagulation and recovery, Water Res. 51 (2014) 113–123.
[23] S. Jagtap, M.K. Yenkie, N. Labhsetwar, S. Rayalu, Fluoride in drinking water and defluoridation of water, Chem. Rev. 112 (2012) 2454–2466.
[24] V. Khatibikamal, A. Torabian, F. Janpoor, G. Hoshyaripour, Fluoride removal from industrial wastewater using electrocoagulation and its adsorption kinetics, J. Hazard. Mater. 179 (2010) 276–280.
[25] J.T. Kloprogge, L.V. Duong, B.J. Wood, R.L. Frost, XPS study of the major minerals in bauxite: Gibbsite, bayerite and (pseudo-)boehmite, J. Colloid Interface Sci. 296 (2006) 572–576.
[26] Y. Ku, H.-M. Chiou, The adsorption of fluoride ion from aqueous solution by activated alumina, Water. Air. Soil Pollut. 133 (2002) 349–361.
[27] M. Kumar, M.N. Babu, T.R. Mankhand, B.D. Pandey, Precipitation of sodium silicofluoride (Na2SiF6) and cryolite (Na3AlF6) from HF/HCl leach liquors of alumino-silicates, Hydrometallurgy 104 (2010) 304–307.
[28] U. Kumari, S.K. Behera, H. Siddiqi, B.C. Meikap, Facile method to synthesize efficient adsorbent from alumina by nitric acid activation: Batch scale defluoridation, kinetics, isotherm studies and implementation on industrial wastewater treatment, J. Hazard. Mater. 381 (2020.) 120917.
[29] G. Lefèvre, M. Duc, M. Fédoroff, Effect of solubility on the determination of the protonable surface site density of oxyhydroxides, J. Colloid Interface Sci. 269 (2004) 274–282.
[30] R. Leyva-Ramos, N.A. Medellin-Castillo, A. Jacobo-Azuara, J. Mendoza-Barron, L.E. Landin-Rodriguez, J.M. Martinez-Rosales, A. Aragon-Piña, Fluoride removal from water solution by adsorption on activated alumina prepared from pseudo-boehmite, J. Env. Eng. Manage 18 (2008) 301–309.
[31] M. Li, T.-C. Hsieh, R.-A. Doong, C.P. Huang, Tuning the adsorption capability of multi-walled carbon nanotubes to polar and non-polar organic compounds by surface oxidation, Sep. Purif. Technol. 117 (2013) 98–103.
[32] J.-Y. Lin, A. Raharjo, L.-H. Hsu, Y.-J. Shih, Y.-H. Huang, Electrocoagulation of tetrafluoroborate (BF_4) and the derived boron and fluorine using aluminum electrodes, Water Res. 155 (2019) 362–371.
[33] S. Meenakshi, N. Viswanathan, Identification of selective ion-exchange resin for fluoride sorption, J. Colloid Interface Sci. 308 (2007) 438–450.
[34] M. Mouelhi, S. Giraudet, A. Amrane, B. Hamrouni, Competitive adsorption of fluoride and natural organic matter onto activated alumina, Environ. Technol. 37 (2016) 2326–2336.
[35] J.P. Nordin, D.J. Sullivan, B.L. Phillips, W.H. Casey, Mechanisms for fluoride-promoted dissolution of bayerite [β-$Al(OH)_{3(s)}$] and boehmite [γ-AlOOH]: ^{19}F-NMR spectroscopy and aqueous surface chemistry, Geochim. Cosmochim. Acta 63 (1999) 3513–3524.
[36] Y. Ren, X. Wei, M. Zhang, Adsorption character for removal Cu(II) by magnetic Cu(II) ion imprinted composite adsorbent, J. Hazard. Mater. 158 (2008) 14–22.
[37] Y. Tang, X. Guan, T. Su, N. Gao, J. Wang, Fluoride adsorption onto activated alumina: Modeling the effects of pH and some competing ions, Colloids Surf. Physicochem. Eng. Asp. 337 (2009) 33–38.
[38] A. Tor, Y. Cengeloglu, M.E. Aydin, M. Ersoz, Removal of phenol from aqueous phase by using neutralized red mud, J. Colloid Interface Sci. 300 (2006) 498–503.
[39] H.N. Tran, S.-J. You, A. Hosseini-Bandegharaei, H.-P. Chao, Mistakes and inconsistencies regarding adsorption of contaminants from aqueous solutions: A critical review, Water Res. 120 (2017) 88–116.
[40] M. Vithanage, A.U. Rajapaksha, M.S. Bootharaju, T. Pradeep, Surface complexation of fluoride at the activated nano-gibbsite water interface, Colloids Surf. Physicochem. Eng. Asp. 462 (2014) 124–130.
[41] D.M. Wang, S.I. Shah, J.G. Chen, C.P. Huang, Catalytic reduction of perchlorate by H2 gas in dilute aqueous solutions, Sep. Purif. Technol. 60 (2008) 14–21.
[42] F. Widhiastuti, J.-Y. Lin, Y.-J. Shih, Y.-H. Huang, Electrocoagulation of boron by electrochemically co-precipitated spinel ferrites, Chem. Eng. J. 350 (2018) 893–901.
[43] C.-H. Won, J. Choi, J. Chung, Evaluation of optimal reuse system for hydrofluoric acid wastewater, J. Hazard. Mater. 239–240 (2012) 110–117.
[44] X. Wu, Y. Zhang, X. Dou, B. Zhao, M. Yang, Fluoride adsorption on an Fe–Al–Ce trimetal hydrous oxide: Characterization of adsorption sites and adsorbed fluorine complex species, Chem. Eng. J. 223 (2013) 364–370.

[45] X. Yang, Z. Sun, D. Wang, W. Forsling, Surface acid–base properties and hydration/dehydration mechanisms of aluminum (hydr)oxides, J. Colloid Interface Sci. 308 (2007) 395–404.
[46] S. Zhang, Y. Lu, X. Lin, X. Su, Y. Zhang, Removal of fluoride from groundwater by adsorption onto La(III)- Al(III) loaded scoria adsorbent, Appl. Surf. Sci. 303 (2014) 1–5.
[47] Y.-X. Zhang, Y. Jia, Fluoride adsorption onto amorphous aluminum hydroxide: Roles of the surface acetate anions, J. Colloid Interface Sci. 483 (2016) 295–306.
[48] T.-T. Zheng, Z.-X. Sun, X.-F. Yang, A. Holmgren, Sorption of phosphate onto mesoporous γ-alumina studied with in-situ ATR-FTIR spectroscopy, Chem. Cent. J. 6 (2012) 419.
[49] V. Žutić, W. Stumm, Effect of organic acids and fluoride on the dissolution kinetics of hydrous alumina. A model study using the rotating disc electrode, Geochim. Cosmochim. Acta 48 (1984) 1493–1503.